Energetics of a Hexagonal–Lamellar–Hexagonal-Phase Transition Sequence in Dioleoylphosphatidylethanolamine Membranes†

Klaus Gawrisch* and V. Adrian Parsegian
DCRT, National Institutes of Health, Bethesda, Maryland 20892
Damian A. Hajduk, Mark W. Tate, and Sol M. Gruner
Physics Department, Princeton University, Princeton, New Jersey 08544-0708
Nola L. Fuller and R. Peter Rand
Biological Sciences, Brock University, St. Catharines, Ontario L2S 3A1, Canada
Received August 30, 1991; Revised Manuscript Received December 17, 1991

ABSTRACT: The phase diagram of DOPE/water dispersions was investigated by NMR and X-ray diffraction in the water concentration range from 2 to 20 water molecules per lipid and in the temperature range from −5 to +50 °C. At temperatures above 22 °C, the dispersions form an inverse (H_{II}) phase at all water concentrations. Below 25 °C, an H_{II} phase occurs at high water concentrations, an L_α phase is formed at intermediate water concentrations, and finally the system switches back to an H_{II} phase at low water concentrations. The enthalpy of the L_α–H_{II}-phase transition is +0.3 kcal/mol as measured by differential scanning calorimetry. Using ^{31}P and ^{2}H NMR and X-ray diffraction, we measured the trapped water volumes in H_{II} and L_α phases as a function of osmotic pressure. The change of the H_{II}-phase free energy as a function of hydration was calculated by integrating the osmotic pressure vs trapped water volume curve. The phase diagram calculated on the basis of the known enthalpy of transition and the osmotic pressure vs water volume curves is in good agreement with the measured one. The H_{II}–L_α–H_{II} double-phase transition at temperatures below 22 °C can be shown to be a consequence of (i) the greater degree of hydration of the H_{II} phase in excess water and (ii) the relative sensitivities with which the lamellar and hexagonal phases dehydrate with increasing osmotic pressure. These results demonstrate the usefulness of osmotic stress measurements to understand lipid-phase diagrams.

The appearance in biological membranes of lipids which promote the formation of nonlamellar phases (Luzzati & Husson, 1962) has led to suggestions of a biological role for these molecules, including involvement in membrane fusion, effects on membrane permeability, and modulation of protein activity. Evaluation of these roles requires knowledge of the elastic properties of the lipid monolayers and of the effects of molecular packing resulting from the inclusion of different lipid types within membranes (Luzzati, 1968; Gruner, 1985; Seddon, 1990; Charvolin, 1990). Quantitative understanding of the magnitude of elastic stress within bilayers is particularly important in deciding if this stress affects protein conformations or facilitates major topological disruptions of membranes during fusion. The most fundamental step toward this understanding for a given system is to determine the phase diagram and to understand the energetics of the various phases. For this reason, we have determined the phase diagram of L-α-dioleoylphosphatidylethanolamine (DOPE),[1] a frequently studied lipid which forms the inverse hexagonal H_{II} phase, and we have measured the enthalpy of the transition between the bilayer L_α and inverted hexagonal H_{II} phases as well as the osmotic work necessary to dehydrate the phases. Although DOPE has been used for nonlamellar investigations for many years, its phase diagram has not been completely determined (Tilcock & Cullis, 1982; Tate & Gruner, 1989; Rand et al., 1990). The diagram turns out to have a number of surprises.

The total free energy of a lipid system is the sum of several energies. In order to focus on mesomorphic phase transitions, Kirk et al. (1984) examined those contributions which are thought to change sharply at the L_α–H_{II}-phase transition. These included a curvature term for the energy of bending a lipid monolayer as well as energies associated with hydration repulsion, electrostatic surface charge, and the constraints of packing hydrocarbon chains.

The free energy change within single-phase regions has been previously examined using osmotic stress techniques. For lamellar phases, the change in energy upon dehydration has been shown to be dominated by the need to overcome an exponential force of hydration repulsion as bilayers are forced together (Rand & Parsegian, 1989). In the H_{II} phase, a change in water content is directly coupled to a change in curvature of the lipid monolayer (Figure 1). Gruner et al. (1986) and Rand et al. (1990) measured the work to dehydrate the H_{II} phase via osmotic methods and attributed that work to a change in the monolayer curvature free energy of the form (Helfrich, 1973)

$$\Delta G = (K_c/2)(1/R - 1/R_0)^2 \quad (1)$$

Here ΔG is the change in free energy per unit area, K_c is the modulus of monolayer stiffness, and R_0 is the spontaneous radius of curvature of the lipid layer.

One must provide a common reference energy, however, for these two free energy forms if one is to understand the energetics of the phase transition. For instance, from eq 1, the

† Work in the Princeton laboratory was supported by grants from the U.S. Department of Energy (DE-FG02-87ER60522), NIH (GM32614), and ONR (N00014-90-J-1702). Work at the Brock laboratory was supported by the Natural Sciences and Engineering Research Council of Canada. K.G. was supported through NIH's Fogarty International Program and D.A.H. by a National Science Foundation graduate fellowship.

[1] Abbreviations: DOPE, L-α-dioleoylphosphatidylethanolamine; PEG, poly(ethylene glycol); H_{II}, inverse hexagonal phase; NMR, nuclear magnetic resonance; DSC, differential scanning calorimetry.

0006-2960/92/0431-2856$03.00/0

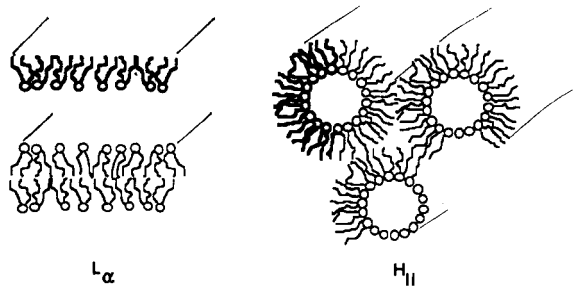

FIGURE 1: Illustration of the configuration of the monolayers of phospholipids in the L_α and H_{II} phases.

lamellar phase with $1/R = 0$ can have an appreciable curvature free energy component if R_0 is finite. Note however that since the curvature changes abruptly at the L_α–H_{II} transition, it is not experimentally possible to verify the form of the curvature free energy over the range of curvatures from infinity to zero. Further, the interaction between lipid monolayers in both phases might be quite different. This is an energy not included in eq 1.

In this paper, the water fraction–temperature phase diagram of DOPE is determined, and the measurement of the work of dehydration is extended to lower water contents and lower temperatures. At sufficiently low temperature, dehydration of DOPE leads to the formation of an L_α phase, in contradiction to the dogma that H_{II} phases always have lower water contents than adjacent L_α phases on the phase diagram. Surprisingly, continued isothermal dehydration results in the reappearance of an H_{II} phase. By use of the Clausius–Clapeyron equation, the calorimetrically determined enthalpy of the H_{II}–L_α-phase transition, and the osmotic pressures necessary to dehydrate lamellar and hexagonal phases, we are able to reconstruct the phase diagram of DOPE including the region of phase coexistence.

Materials and Methods

Synthetic L-α-dioleoylphosphatidylethanolamine (DOPE) purchased from Avanti Polar Lipids Inc., Alabaster, AL, was used without further purification. The lipid was checked for impurities by thin-layer chromatography and was judged to be at least 98% pure. Poly(ethylene glycol) (Carbowax 20000; Fluka, Buchs, Switzerland) was used to prepare osmotic stress solutions.

NMR. NMR measurements were performed on a Bruker MSL 300 spectrometer (Karlsruhe, Germany), using a high-power probe with an 8-mm solenoidal sample coil which was doubly tuned for ^{31}P and ^{1}H at 121.513 and 300.133 MHz, respectively. Gated broad-band-decoupled ^{31}P spectra were observed with a phase-cycled Hahn echo sequence as described by Rance and Byrd (1983). A delay time between the 90° and 180° pulses of 100 μs was chosen. Typically, 1024 scans with a recycle delay time of 1 s were accumulated. No significant intensity or line-shape change was observed after an increase of the recycle delay time. ^{2}H NMR spectra were observed using the same 8-mm solenoidal sample coil as for ^{31}P NMR but tuned for a resonance at 46.073 MHz. Tuning was possible without removal of the sample from the probehead. ^{2}H NMR spectra were obtained using a quadrupole echo sequence with phase cycling as described by Davis et al. (1976). An interpulse delay of 100 μs and a recycle delay of 250 ms or 1 s were chosen. Part of the spectra was obtained by accumulation of the free induction decay after a single 60° pulse with quadrature detection phase cycling.

The appropriate sample temperature (±0.5 °C) in the NMR experiments was adjusted by a Bruker temperature-control unit. The probe temperature was measured by a digital thermometer with the sensor placed close to the solenoid coil. Samples were equilibrated at the appropriate temperature in a thermostat/cryostat for several days before the measurements. They were immediately transferred to the spectrometer without any change in temperature. Measurements on a particular sample as a function of temperature were performed in jumps of 2 °C per hour (samples containing 4, 18, and more water molecules per lipid) or 2 °C per 15 min (9–12 water molecules per lipid).

For data analysis, part of the NMR spectra was transferred from the Aspect 3000 computer of the MSL 300 spectrometer to an IBM AT-compatible computer using a Kermit protocol. Intensities of overlapping resonance lines of different phases were determined by a line-shape fitting procedure, using the sum of mean square deviations between measured and calculated intensities as an indicator for the quality of the fit. The relative intensities of both phases, the anisotropies of chemical shift, and the line widths of resonance lines can be chosen as variable parameters in the fit procedure. Reasonable starting values were obtained from comparison of the experimental spectra with a set of calculated spectra.

Two kinds of lipid samples were prepared for NMR. "Gravimetric samples" were prepared by adding known amounts of water to anhydrous lipid. Before sample preparation, the lipids were dried for at least 24 h over P_2O_5 in an evacuated desiccator. Between 50 and 100 mg of the lipid was put into short sample tubes of 8-mm diameter in a glovebag filled with dry nitrogen. The exact amount of lipid was determined with balances in the glovebag. The glass tubes were then sealed with Parafilm. Low paramagnetic deuterium oxide, 99.6% deuterated (Cambridge Isotope Laboratories, Woburn, MA), was added with a microsyringe by puncturing the Parafilm. The amount of added water was then determined by weight.

To prevent evaporation or condensation of water, the glass tubes were put into dry nitrogen filled 2-mL plastic vials topped with screwcaps with O-ring seals. The sample contents were then pelleted by centrifugation. Before the NMR measurements, the samples were stored for at least several days at room temperature and after that for at least 2 days at the temperature of investigation.

A second set of gravimetric samples was prepared in glass tubes filled with dry nitrogen. Water was added through a constriction in the tubes which was flame-sealed afterward. The sample contents were homogenized by centrifuging the contents up and down the tubes.

Another kind of NMR sample, called "PEG samples", consisted of lipid in osmotic equilibrium with poly(ethylene glycol) (PEG) solutions of known osmotic pressures (Parsegian et al., 1986; Gawrisch et al., 1988). About 50 mg of prehydrated DOPE was dispersed in 2 mL of PEG/water solution and kept for at least a day at room temperature. The samples were stirred on a Vortex mixer several times to prevent formation of water concentration gradients in the PEG solution. Before the measurements, the lipid was pelleted by centrifugation, removed from most of the PEG/water solution with a spatula, and placed in glass tubes, after which the samples were cooled to the appropriate temperature.

X-ray Diffraction. X-ray samples were produced by weighing the dry lipid and 2 mM TES buffer (pH 7.3) into small weighing bottles and equilibrating in the dark, at room temperature, for 48 h, or by equilibrating with PEG solutions of measured osmotic pressure or with vapors of saturated salt solutions of known vapor pressure (Parsegian et al., 1986). No

water loss was detected before the hydrated lipid was mounted into X-ray sample holders at the equilibrating temperature. Each sample was combined with some powdered Teflon (as an X-ray calibration standard) and sealed between mica windows 1 mm apart.

X-ray diffraction was used to characterize the structures and their dimensions that were formed by the various lipid mixtures. X-ray measurements were performed on either of two small-angle X-ray diffraction facilities as previously described (Rand et al., 1990; Tate & Gruner, 1989). A lamellar phase was characterized by a series of three to five X-ray line spacings in the ratios of the unit-cell dimension, d_{lam}, of 1/1, 1/2, 1/3, 1/4, etc. A hexagonal phase was characterized by X-ray spacings bearing ratios to the dimension of the first order, d_{hex}, of 1, $1/\sqrt{3}$, $1/\sqrt{4}$, $1/\sqrt{7}$, etc. Coexistence of lamellar and hexagonal phases appeared as coexistence of the lamellar and hexagonal series of reflections.

For a single hexagonal or lamellar phase of known composition, the unit cell can be divided into lipid and aqueous compartments and molecular dimensions calculated as described in detail recently (Rand et al., 1990). For the lamellar phase the molecular area, A, projected onto a plane perpendicular to the bilayer normal, the bilayer thickness, d_l, and the bilayer separation, d_w, were determined. For the hexagonal phases, it has been assumed that the water cores are circular in cross section, an assumption shown to be valid in the case of DOPE (Turner & Gruner, 1989; 1991; Turner, 1990). In the hexagonal structure, the average molecular area projected onto a surface parallel to the axis of the water core depends strongly on the distance of that surface from that axis. Here it is calculated at two positions: at radius R_w, the lipid–water interface, as A_w; and at the ends of the hydrocarbon chains, as A_t. It can be determined at intermediate positions of the molecule by including part of the volume of the lipid molecule within the cylindrical surface (Rand et al., 1990).

DSC. Differential scanning calorimetry was performed on DSC-2 (Perkin-Elmer Corp., Norwalk, CT) and Privalov-DASM-4 (Mashpriborintorg, Poushtchino, Russia) calorimeters. Samples for the DSC-2 were prepared in aluminum DSC pans. The weight of the dry lipid (≈2 mg) was determined by electrobalances with an accuracy of ±0.01 mg. Water was added in excess. Samples were equilibrated for 24 h at room temperature before the measurements. On the DSC-2, the heats of lamellar–hexagonal transitions were calibrated against the known heat of the "main" transition at 41.5 °C for melting of the lipid hydrocarbon chains of dipalmitoylphosphatidylcholine (Mabrey & Sturtevant, 1976). Samples for the DASM-4 contained about 10 mg of DOPE/mL of doubly distilled water. Samples were homogenized by several freeze–thaw cycles. The calorimeter was cooled to +1 °C, and the cold sample was filled into the calorimeter capillary. Enthalpies were calculated from computer-integrated peak areas using built-in calibrated heat sources of the DASM-4.

Results

The Phase Diagram. NMR was found to be an excellent method to determine the amount of lipid and water in coexisting lamellar and hexagonal phases. Provided that there is a reasonable signal-to-noise-ratio in the NMR spectra and that the lipid is not orienting under the influence of the strong applied magnetic field, the observed line shape can easily be decomposed into contributions from each phase. Base-line distortions and phase errors in the spectra were minimized by using echo sequences. The T_2 relaxation times of lipid phosphate signals and of deuterated water signals were of the order of milliseconds. A delay time of 100 μs between the pulses in the echo sequences was optimal to prevent base-line distortions and caused no observable line-shape changes due to relaxation.

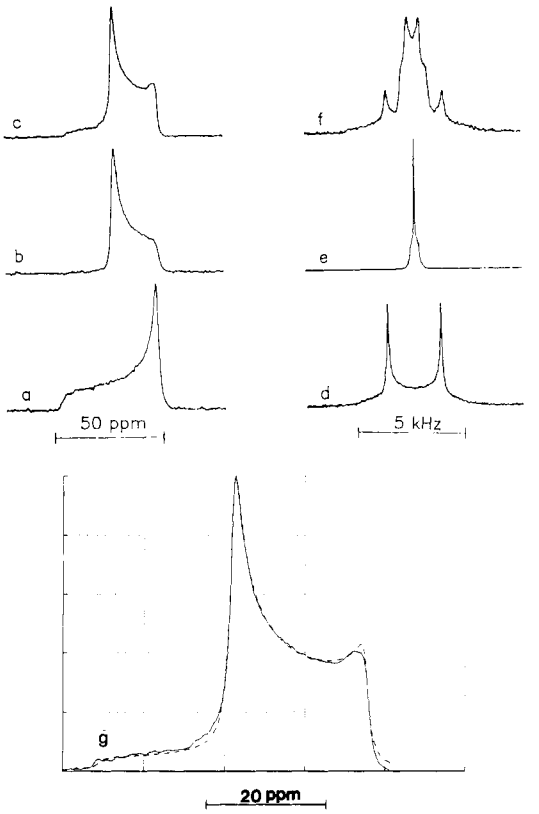

FIGURE 2: ^{31}P NMR spectra of DOPE in lamellar and hexagonal phases. (a) Lamellar phase, 9.7 waters/lipid (n_w = 9.7), T = 14 °C, $\Delta\sigma$ = −43.5 ppm. (b) Hexagonal phase, n_w = 20, T = 14 °C, $\Delta\sigma$ = 20.7 ppm. (c) Mixture of hexagonal and lamellar phases, n_w = 8, T = 20 °C, $\Delta\sigma_{lam}$ = −41.0 ppm, $\Delta\sigma_{hex}$ = +20.5 ppm, intensities 29% lamellar, 71% hexagonal. (d–f) ^2H NMR spectra of ^2H_2O in lamellar and hexagonal phases, samples as in spectra a–c: (d) n_w = 9.7, $\Delta\nu_Q$ = 2.5 kHz, T = 14 °C; (e) n_w = 20, T = 14 °C; (f) n_w = 8, T = 20 °C, $\Delta\nu_{Q,lam}$ = 2.77 kHz. (g) Fit of line shape of spectrum c: (—) experimental spectrum; (- - -) calculated spectrum. Except for possible orientational effects of applied magnetic fields, the NMR spectra are easily interpreted in terms of symmetry of motions of the lipid molecules in the respective phases.

Signal decomposition was performed using a computer program as described in Figure 2. The accuracy of the relative intensities determined in regions of coexistence of lamellar and hexagonal phases was most seriously affected by a preferred lipid orientation caused by the 7-T magnetic field. The influence of magnetic field induced orientation could be easily checked by turning the sample 90° in the solenoid coil. Usually, orientational effects became more important after several hours of measurements with cycling of the sample temperature. In the H_{II} phase below room temperature and at concentrations of about four waters per lipid, the expected fast reorientation of lipid molecules around the hexagonal cylinder axes became slower and caused significant intensity changes in the spectra. The strong temperature dependence of these changes in line shape may be used to calculate a diffusion constant of lipid molecules moving around the long axis of the cylinder. These data will be presented in a separate paper. Spectra recorded in a narrow temperature interval around 6 °C for the sample containing four waters per lipid showed an additional intensity at the isotropic position. This is in agreement with the detection of another phase (possibly cubic) by X-ray diffraction (see below).

As with the lipid molecules in ^{31}P NMR, some of the ^2H_2O molecules in ^2H NMR show distinguishable signals for lamellar and hexagonal phases. Usually this water in the lamellar phase has a sharp quadrupolar splitting while the water in the hexagonal phase has an unresolved splitting which is less than half of that of the lamellar phase. Water spectra of the hexagonal phase can be fitted by a superposition of a broadened quadrupolar split spectrum plus a broadened isotropic water signal of low intensity.

While the quadrupolar splitting of water in the lamellar phase is a strong function of water concentration, the poorly resolved quadrupolar splitting of the hexagonal phase is not. The line shape of the ^2H NMR resonance lines of ^2H_2O in the hexagonal phase is certainly the result of a slow exchange between sites of different orientation. Because of the high diffusion rate of water in lipids ($D = 10^{-6}$ cm^2/s; Rigaud et al., 1972), the distance between these sites can be up to a micrometer. The superstructure of cylinder packing in hexagonal phases, i.e., the fact that the H_{II} cylinders are not perfectly straight (Gruner et al., 1982), is a likely candidate to explain the behavior. The sensitivity of the line shape to the sample preparation procedure supports this view. Recently, we confirmed this interpretation by the investigation of hexagonal phases oriented between glass plates. If the long axis of the hexagonal-phase cylinders is oriented perpendicular to the magnetic field, a bending of cylinders in a plane perpendicular to the magnetic field is not going to change the effective orientation of the motionally averaged electric field gradients of water molecules with respect to the magnetic field. In good agreement with this prediction, unperturbed sharp doublets of water in hexagonal phases, oriented as described above, were observed.

The phase state as a function of temperature of samples containing 4, 9–12, 18, and 38 water molecules per lipid was investigated with NMR. Samples containing four water molecules per lipid were in a hexagonal phase down to temperatures of about 7 °C. A lamellar phase was observed below 2 °C. The phase state between 7 and 2 °C has not been identified with certainty. The highest phase transition temperature (22 °C) from an H_{II} to an L_α phase was observed with samples containing about 10 water molecules per lipid. If the water concentration was ±1 water molecule different from 10, the phase transition temperature was about 3 °C lower. Also, the width of the transition (about 4 °C) increased significantly with increasing and decreasing water concentrations (6 °C and more). This behavior poses serious obstacles to locating sharp boundaries on phase diagrams. Operationally, a single-phase region was defined as one in which greater than about 90% of the lipid was in a single phase. No hysteresis between heating and cooling scans was observed for samples containing from 9 to 12 water molecules per lipid, in sharp contrast to samples containing 18 or more water molecules per lipid. Upon being cooled, these latter samples entered a lamellar phase at temperatures between 0 and −3 °C. Upon being heated, the phase transition back to the hexagonal phase occurred at about 6 °C. The transition temperatures were dependent on the thermal history of the sample. Worse still, at temperatures at which the L_α and H_{II} structures were observed in coexistence, the amounts of lipid in both forms changed slowly over a longer time.

Lamellar samples containing 18 water molecules per lipid showed an isotropic 100-Hz-wide ^2H NMR water signal superimposed on a signal split by a quadrupolar interaction (Figure 3). An integration indicated that the split signal accounts for 11 ± 1 out of 18 water molecules added. The central peak arises from water molecules which execute isotropic diffusive motion on the NMR time scale. In addition to free water, isotropic motion may occur if the water performs diffusive motion over the surface of small liposomes. At least some of the water must be free water for the following reasons: (1) Tiny water droplets are seen to collect on the tube walls above the lipid mass when the lipid is in the L_α phase. They disappear during the L_α–H_{II}-phase transition. (2) As described below, the lamellar X-ray repeat spacing reaches a maximum at 11 waters per lipid. Saturation of the repeat spacing has traditionally been taken as a definition of the excess water point of a lamellar phase. (3) The ^{31}P NMR signal of lipids shows no indications of highly curved lipid bilayers. However, ^{31}P NMR is less sensitive to curvature because of the lower lateral diffusion rate of lipids in comparison with water. (4) The quadrupolar splitting of the signal (2.1 kHz) was within experimental error identical to the quadrupolar splitting of samples which contained about 12 water molecules per lipid at the same temperature. These results indicate that the maximum amount of water in a L_α phase of DOPE at 0 °C is about 11 ± 1 water molecules per lipid. The different water uptake of DOPE in hexagonal and lamellar phases in excess water could explain the time-dependent hysteresis of the H_{II}–L_α-phase transition between heating and cooling scans.

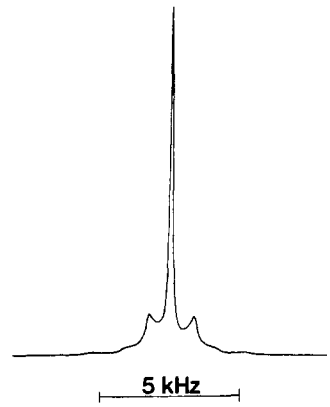

FIGURE 3: ^2H NMR spectrum of deuterated water in a sample containing 18.2 water molecules per DOPE at 3 °C (lamellar phase). The signal split by a quadrupolar interaction is caused by water in the lamellar phase. The superimposed isotropic signal is free water which left the lipid phase during the H_{II}–L_α-phase transition. The ratio of intensities of both spectra corresponds to a water concentration of 11 ± 1 water molecules per DOPE in the lamellar phase.

A set of gravimetric samples, containing from 2 to 15 water molecules per lipid, was investigated at 20 and 14 °C. To obtain reproducible results, all samples were cooled from higher temperatures to the temperature of the experiment and stored for several days. At both temperatures, the samples form a single hexagonal phase in excess water, then enter a lamellar phase with dehydration, and finally reenter a hexagonal phase with further dehydration. There is a coexistence of lamellar and hexagonal phases over a certain water concentration range. In Figure 4, the proportion of DOPE in the lamellar phase is given as a function of water concentration, as determined by ^{31}P NMR measurements. The region of existence of the lamellar phase broadens with a lowering of the sample temperature.

A phase diagram was also determined by X-ray diffraction and is shown in Figure 5. The X-ray and NMR-phase assignments agree to within the temperature sampling shown, including the reentrant lamellar- and hexagonal-phase boundaries. Figure 5 also shows a narrow region near the low-water, low-temperature side of the L_α phase where X-ray lines were observed in the ratio to the dimension of the first

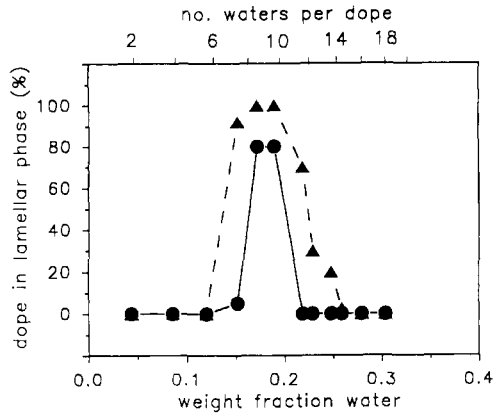

FIGURE 4: Mole fraction of total lipid DOPE in the lamellar phase as a function of water concentration at 20 (●) and 14 °C (▲). While at 20 °C, only two samples showed detectable amounts of lamellar phase; at 14 °C, the lamellar structure was seen over a broad range of water contents. The 14 °C samples with 9–10 water molecules per phospholipid were 100% lamellar. The occurrence of L_α structure at these temperatures is eradicated by the addition of small amounts of dodecane.

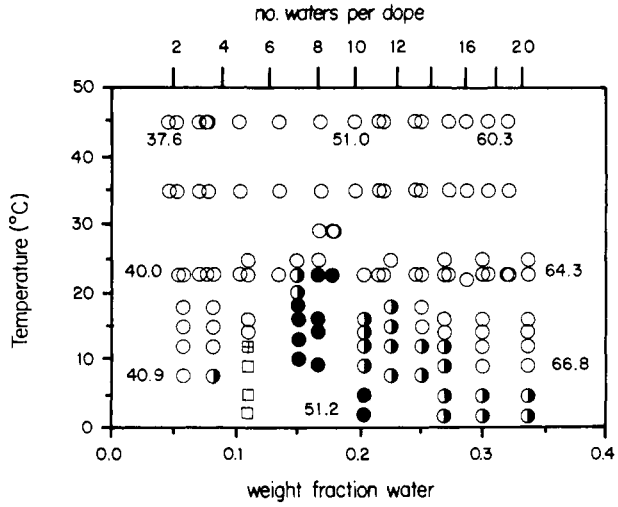

FIGURE 5: Phase diagram of DOPE as a function of temperature and water concentration as determined by X-ray diffraction. The numbers in the graph are representative lamellar and hexagonal lattice spacings. The cubic lattice assignments are based on only a few peaks and, therefore, should be considered tentative. An azeotrope point (the point at which the L_α and H_{II} phases have identical volume fractions of water) occurs at about 22 °C and 10 waters per phospholipid. No lamellar phase is observed above 22 °C. (○) Hexagonal; (●) lamellar; (◑) lamellar + hexagonal; (□) cubic; (⊞) cubic + hexagonal.

order of $\sqrt{2}/\sqrt{3}/\sqrt{5}/\sqrt{8}$, which characterizes neither lamellar nor hexagonal lattices. The X-ray patterns showed many sharp spots at low angle, indicative of large crystallites frequently seen with cubic phases.

The NMR measurements involved DOPE dispersed in ^2H_2O while X-ray and calorimetric measurements were performed with H_2O dispersions. X-ray investigations were performed to determine if there were differences between excess water H_2O and ^2H_2O dispersions which were subjected to identical temperature variation protocols. The H_2O and ^2H_2O specimens exhibited the same lattice spacings (to within ±0.5 Å) in excess water when both samples were in a given phase at a given temperature. The L_α–H_{II} transition temperature for the ^2H_2O specimens was systematically lower by about 1–3 °C; however, this shift is below the resolution of the temperature samplings of the phase diagram in Figure 5.

Representative lamellar and hexagonal lattice spacings are shown in Figure 5. The methods described in Rand et al.

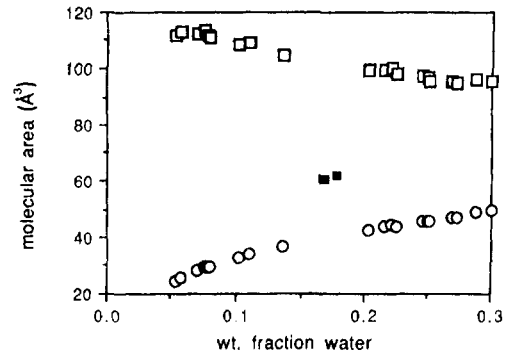

FIGURE 6: Area available per DOPE lipid molecule at 22.5 °C as the water content of the phases changes. For the hexagonal phase, the area is calculated both at the polar group–water interface (○) and at the terminal methyl ends of the hydrocarbon chains (□). This latter area is defined as an average area per molecule on the Wigner–Seitz cell boundary and, thus, is independent of any assumptions about the shape of the cross section of the water cylinder. The polar ends are compressed with dehydration while the hydrocarbon ends are dilated. The area available per lipid molecule projected onto the plane perpendicular to the bilayer normal for the intervening lamellar phase is also given (■). At the H_{II} to L_α transition, the polar group area abruptly increases, and the hydrocarbon area abruptly decreases.

(1990) can be used to calculate a number of molecular dimensions and how these change with water content. According to the dependence of the lamellar repeat spacing as a function of water concentration, the hydration of the lamellar phase reaches a maximum at about 11 waters per molecule while the hexagonal phase has a maximum hydration of about 18 water molecules per lipid at 22 °C. These numbers will be used for the calculation of the DOPE phase diagram. Figure 6 shows molecular areas measured at 22 °C. Upon dehydration, the molecular area at the lipid headgroup decreases while the area at the other (terminal chain methyl) end of the molecule increases. Since the changes in area have opposite signs, there must be some "pivotal" position within the depth of the monolayer (Rand et al., 1990) where there is no net change in molecular cross-sectional area, at least for a limited range of dehydration. Figure 6 shows that the cross-sectional molecular area in the lamellar phase, which is, by definition, uniform throughout the thickness of the bilayer, is about 60 Å^2. That area is intermediate between the molecular areas at each end of the phospholipid molecule when it is in the hexagonal phase.

Finally, addition of 5 lipid wt % dodecane completely abolishes the formation of the lamellar phase upon dehydration, suggesting that hydrocarbon packing effects are significant (Gruner, 1989).

Osmotic Stress of the DOPE Phases. The volume of trapped water in lamellar and hexagonal phases of DOPE as a function of osmotic stress was measured by NMR for the lamellar phase (Arnold et al., 1983; Gawrisch et al., 1988) and by X-ray diffraction for the hexagonal phase (Rand et al., 1990).

Figure 7 shows ^{31}P and ^2H NMR spectra of lipid samples equilibrated with two different osmotic pressures of the PEG-20 000/water solution. If there is no interaction between the PEG molecules and the lipid, osmotic equilibration with PEG solutions allows sensitive control of the water concentration in the lipid. As expected, the lipid is in a hexagonal phase at low PEG concentrations but then enters a lamellar phase at intermediate concentrations and switches back to the hexagonal state at very high concentrations. Because the limited solubility of PEG in water limits the attainable osmotic pressure, reentrance into the hexagonal phase is not usually fully achieved with PEG solutions if the temperature is too

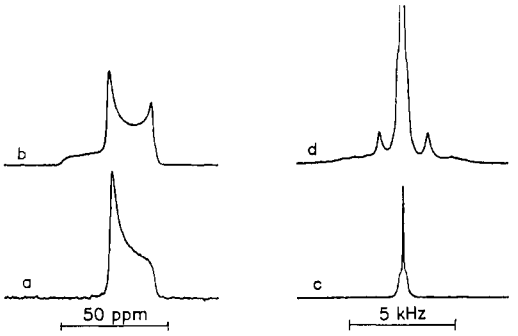

FIGURE 7: ^{31}P and ^{2}P NMR spectra of DOPE/$^{2}H_2O$ dispersions in solutions of PEG 20 000 at 20 °C. (a) ^{31}P NMR, 20 wt % PEG, log P = 6.88 (P in dyn/cm^2). (b) ^{31}P NMR, 40 wt % PEG, log P = 7.72 (P in dyn/cm^2). (c) ^{2}H NMR, 20 wt % PEG. (d) ^{2}H NMR, 40 wt % PEG. At low PEG concentrations, DOPE is in a hexagonal phase; at intermediate concentrations, a lamellar phase coexists with a hexagonal phase and then (not shown) at high osmotic stress (or low vapor pressure) a single hexagonal phase exists.

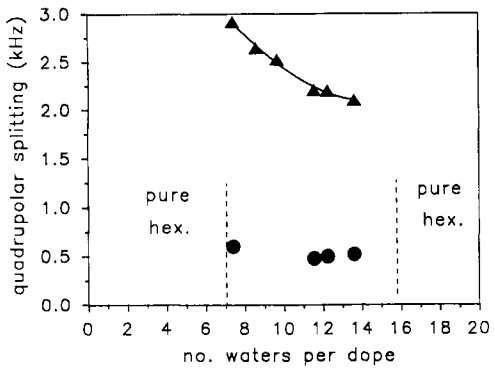

FIGURE 8: Quadrupolar splitting of deuterated water in DOPE/$^{2}H_2O$ dispersions at 14 °C as a function of water content. At around 10 waters per phospholipid, there is a pure lamellar phase. Dehydration of this phase results in an increased quadrupolar splitting of the $^{2}H_2O$ signal down to a content of 7 waters per lipid at which point there is a total reversion to the H_{II} structure. (▲) Lamellar phase; (●) hexagonal phase.

much below 20 °C, but can be reached by reduced water vapor pressures. There is a coexistence of both phases over a narrow PEG concentration region.

The existence of a lamellar phase at intermediate PEG concentrations not only is reflected by ^{31}P NMR but also is visible in the ^{2}H NMR spectra of deuterated water (Figure 7). The significantly broader quadrupolar-split spectra of the lamellar phase are superimposed on the spectra of the isotropic water of the PEG/water solution and the narrower splitting of the hexagonal phase if present.

The quadrupolar splitting of water between lipid bilayers increases with increasing osmotic pressure (Figure 9). Using Figure 8, which shows the corresponding quadrupolar splittings for gravimetrically prepared samples and assuming a volume of 30 Å^3 per water molecule, these splittings can be used to calculate a volume of water per lipid molecule. That combination then produces the relation between osmotic pressure and volume of water per lipid molecule. This is shown in Figure 10 for lipid at 14 °C where a lamellar phase exists for PEG solutions between 30 and 50 wt %.

The equilibrated osmotic pressure, P, in most lamellar lipid systems (Rand & Parsegian, 1989) varies with the water volume/lipid, V_w, as

$$P = P_0 \exp(-V_w/\mu) \qquad (2)$$

Hence, a plot of log P vs V_w yields both P and μ. A least-squares fit (dashed line, Figure 10) gives $P_0 = 10^{9.2\pm0.6}$ dyn/cm^2

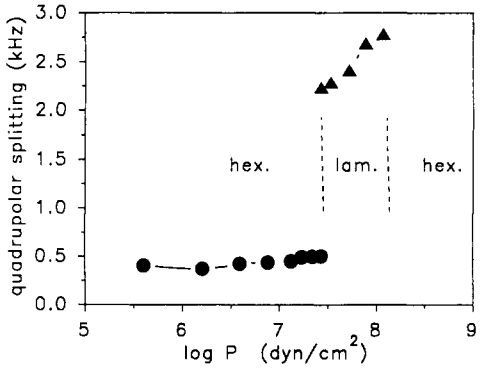

FIGURE 9: $^{2}H_2O$ quadrupolar splitting as a function of osmotic stress exerted by PEG on the lamellar or the hexagonal lattice. The monotonic relation seen with the lamellar phase, combined with the splitting vs water content of Figure 8, allows one to construct the osmotic stress vs water volume given in Figure 10. A volume of 30 Å^3 per water molecule was assumed.

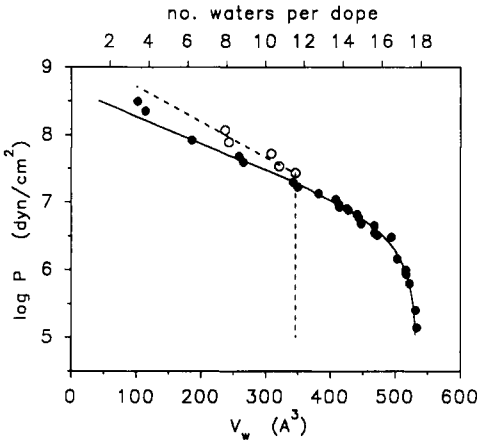

FIGURE 10: Osmotic stress vs water volume for the lamellar and hexagonal phases of DOPE at 14 and 22 °C, respectively. The data for the lamellar phase (○) can be fitted by $P_l = P_0 \exp(-V_w/\mu)$, where $P_0 = 10^{9.2}$ erg/cm^3 and μ = 85 Å^3. This relation may be used to infer the rate of change of the free energy of the DOPE lamellar phase. The data for the hexagonal phase (●) were fitted by a polynomial function: $\log P_h = (1.43894 \times 10^4) - (1.59369 \times 10^2)V_w + (7.04931 \times 10^{-1})V_w^2 - (1.55586 \times 10^{-3})V_w^3 + (1.71351 \times 10^{-6})V_w^4 - (7.53388 \times 10^{-10})V_w^5$ for values of $\log P_h \leq 7$ and by $\log P_h = 8.6755 - (4.0413 \times 10^{-3})V_w$ for values of $\log P_h > 7$.

and $\mu = 85 \pm 20$ Å^3. The rather large errors associated with this fit arise primarily because the fit to log P is over a small span in V_w. The fitted line in Figure 10 is shown extrapolated to values of V_w of 330 Å^3, which corresponds to the maximum swelling of bilayers observed for gravimetric samples.

The measurement of trapped water in the hexagonal phase as a function of osmotic stress was performed at 22.5 °C (Figure 10, solid line). While the water volume determination for the lamellar phase proved to be more accurate using the ^{2}H NMR quadrupolar splitting of deuterated water, the trapped water volume in the hexagonal phase could be determined with higher resolution by X-ray diffraction [see Rand et al. (1990) for details]. The repeat spacing of the hexagonal phase was compared with the repeat spacing of gravimetric samples of known composition.

DSC Measurements. The sensitivity of the H_{II}–L_α-phase transition to osmotic work suggests that one may relate the change in transition temperature to the applied osmotic stress. In anticipation of a connection between the osmotic work and the heat of transition (see the Discussion), we measured the heat of transition for both the hexagonal–lamellar- and lamellar–hexagonal-phase transitions for DOPE in excess water. The calorimetry measurements show that there is an uptake

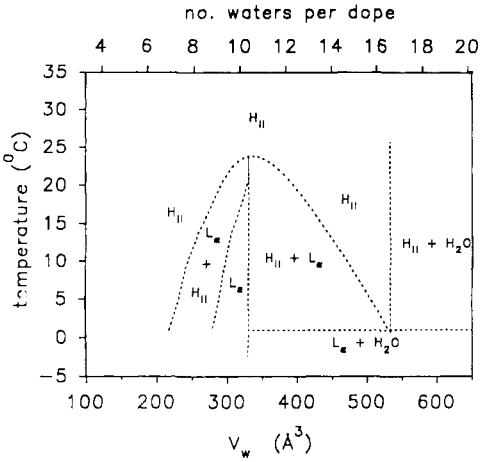

FIGURE 11: Calculated phase diagram of DOPE as a function of water concentration and temperature. The calculation uses the osmotic pressure/volume functions of Figure 10, the enthalpy of the H_{II}–L_α-phase transition (0.3 kcal/mol), and the transition temperature in excess water (+1 °C).

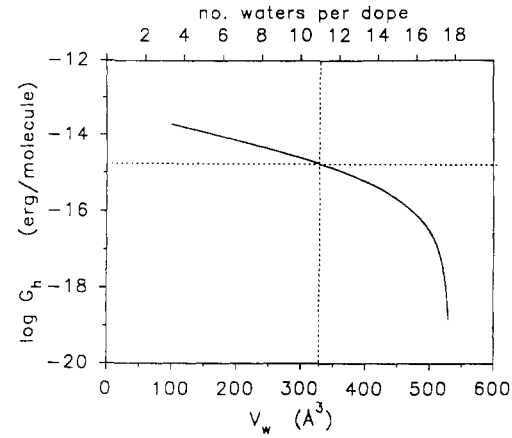

FIGURE 12: Computed free energy of DOPE vs water content in the H_{II} phase at 22 °C. At a water concentration close to 11 water molcules per lipid (V_w = 330 Å^3; dotted lines), a narrow region of coexistence of lamellar and hexagonal phases was observed. An osmotic work of the order of 0.05 kT (see eq 5) has to be performed to transform a hexagonal phase in excess water to a hexagonal phase which has the same free energy as a lamellar phase.

of a latent heat going from the lamellar to the hexagonal phase. The measurements were performed at heating rates of 5, 1.25, and 0.125 °C/min. The temperature of the peak in the DSC scan strongly depended on the heating or cooling rate, but the magnitude of the heat of transition, 0.30 ± 0.05 kcal/mol, was independent of hysteresis effects. These measurements agree with data previously reported (Wistrom et al., 1989; Epand, 1985).

Discussion

Reconstruction of the Phase Diagram. The L_α–H_{II} transition studied here is first order and is associated with discrete changes in enthalpy, ΔH, and in volume, ΔV, of water per lipid. Since the measurements are at constant (atmospheric) pressure, density differences between the two forms are not at issue. These changes in the extensive parameters of the system are related to the phase coexistence line by the Clausius–Clapeyron relation:

$$\frac{dP}{dT_{LH}} = \frac{\Delta H}{T_{LH}\Delta V} \tag{3}$$

where P is the osmotic pressure and T_{LH} is the transition temperature. According to eq 3, the application of osmotic stress at constant temperature shifts the phase transition toward the phase with the lower water content. One may use eq 3 to reconstruct the phase diagram if ΔH and ΔV are known along the phase coexistence curve.

By making two simplifying assumptions concerning ΔH and ΔV, important insights into the nature of the DOPE/water system can be gained. First, we will assume that ΔH is constant along the phase transition line. Second, we assume that the osmotic stress curves of Figure 10 are independent of temperature, making ΔV independent of temperature as well. Using eq 3, several features of the phase diagram become immediately obvious. Below an osmotic pressure of 2×10^7 dyn/cm^2, the lamellar phase has a lower water content, and the phase transition temperature, T_{LH}, should rise. Above this pressure, the H_{II} phase has fewer water molecules per lipid and T_{LH} falls. At 2×10^7 dyn/cm^2, there is no change in water volume across the phase transition. This point is known as the azeotrope point and will be the point where T_{LH} is maximum. Integrating eq 3, we obtain

$$T_{LH} = T_0 + \frac{T_0}{\Delta H}\int_0^P \Delta V\, dP \tag{4}$$

where T_0 is the phase transition temperature in excess water. Figure 11 shows the calculated phase diagram using this equation, with T_0 taken to be 1 °C, an average of transition temperatures found for heating and cooling scans. This figure has the same qualitative features as the measured phase diagram of Figure 4. It also shows surprising quantitative agreement considering the simplifying assumptions made above.

Refining the values used for ΔH and ΔV will, of course, improve the calculated phase diagram. In particular, it is known that the amount of water per lipid molecule incorporated into the hexagonal phase changes by two water molecules per lipid over the temperature range from 10 to 35 °C (Tate & Gruner, 1989). In addition, the measurement of an equilibrium phase diagram is complicated by the presence of slow, power-law kinetics which broaden the phase coexistence region (Tate et al., 1991). The above calculation does however highlight several salient features of the DOPE/water phase diagram: (i) in excess water, the hexagonal phase must take up more water than the lamellar phase; (ii) the H_{II} phase must be more easily dehydrated.

Energy Changes. The osmotic stress technique allows direct measurements of the change in the total free energy upon dehydration by integrating over the water volume change:

$$\Delta G = \int_{V_{w0}}^{V_w} P\, dV_w \tag{5}$$

Figure 12 shows the change in free energy for the hexagonal phase at the azeotrope temperature, 22 °C. Plotted on a logarithmic scale, this energy is convex upward, reaching a value of about 1.8×10^{-15} erg/molecule $\approx$ 0.05 kT when dehydrated to the azeotrope volume.

X-ray diffraction of DOPE H_{II} phases at room temperature shows that the pressure vs radius of curvature can be fitted, over an approximately 2-fold range of curvatures, by the form

$$P = K_0(1/R - 1/R_0)(-1/R^2)/(A/2) \tag{6}$$

which is derived from the bending energy of eq 1 (Rand et al., 1990). Here, K_0 is the monolayer elastic bending modulus, R is the radius of a pivotal surface which characterizes the radius of curvature of the monolayer in the hexagonal phase, and A is the cross-sectional molecular area at radius R. The pivotal surface is defined as the position of the cylindrical

surface, parallel to the lipid/water interface, which partitions the volume of the lipid molecule in such a way that the area per lipid changes least with bending of the layer. R_0 is about equal to the value of the pivotal surface in excess water. Note that as the monolayer is bent, the molecular area on the polar group side decreases while on the hydrocarbon chain side of the pivotal surface the molecular area increases (Figure 6). For practical purposes, it is useful to introduce the modulus $K_c = 2K_0/A$ to convert an energy per molecule to an energy per area. The factor of 2 is necessary for a comparison with bilayers.

After Kirk et al. (1984), we assume that the flattening of a hexagonal-phase monolayer of radius R into a lamellar configuration increases the associated bending free energy by $K_c/2R_0^2$. Using the fitted values for DOPE of K_c = 42.5 kT and R_0 = 31 Å, we obtain an energy of 1.6 kT/molecule = 6.6×10^{-14} erg. Since the change of the total free energy across the phase transition is zero, there must exist some competing free energy which favors the lamellar phase.

One could list many factors to account for the 1.6 kT/molecule energy difference. There may be additional energies associated with the interaction of apposing monolayers at the terminal ends of the acyl chains, especially since the molecular areas are so different in the two phases (Figure 6). Monolayer bending may involve both bending and lateral compression. Recently, a more general fitting procedure of the free energy of the hexagonal phase (Figure 12) was suggested by Kozlov and Winterhalter (1991a,b) which takes into account both a bending and a lateral compressibility. Lateral compressibility can be very different at polar and at hydrocarbon regions. The L_α–H_{II}-phase transition is sensitive to changes in both the polar region and the hydrophobic regions of phospholipid molecules (see Conclusions for details).

Whatever the exact value of the bending energy may be, there must be competing free energy components so that the net change in free energy across the L_α–H_{II} boundary is zero. Kirk et al. (1984) considered the unfavorable situation associated with the anisotropic packing of hydrocarbon chains in the H_{II} geometry. This anisotropy would lower the configurational entropy of the chains, and hence raise the free energy of the H_{II} phase. If a small quantity of free alkane partitioned so as to lower this packing anisotropy, the free energy of the H_{II} phase would be lowered, reducing or eliminating the L_α phase (Kirk & Gruner, 1985). Here again we show a similar effect for a system under osmotic stress, indicating that in addition to headgroup effects, chain packing considerations play a large role in the determination of the equilibrium phase.

Conclusions

At sufficiently high temperatures, DOPE assembles into an H_{II} phase over a wide range of water concentrations. At lower temperatures besides the H_{II} phase, other phases, including L_α and possibly cubic phases, are observed. A particularly interesting aspect of the phase diagram is that at these lower temperatures, the H_{II} phase is reentrant upon isothermal dehydration, transforming from H_{II} to L_α and back to H_{II}. A transition from hexagonal to lamellar structures induced by the addition of the dehydrating agent PEG was reported earlier by Boni et al. (1984). The observation of an H_{II}- to L_α-phase transition upon dehydration is otherwise counter to previously reported transformations in diacylphospholipid systems. However, a simple consequence of the Clausius–Clapeyron equation is that such behavior should be present in any system for which the H_{II} phase is more hydrated than the lamellar phase. The transition back to the H_{II} phase upon further dehydration is a consequence of the slower growth in the H_{II} free energy compared to the more rapid exponential growth of the lamellar energy.

Consistent with its low enthalpy, 0.3 kcal/mol, and its temperature sensitivity, the H_{II}–L_α transition requires little osmotic work. This is indicated by the observation that the transition temperature changes by over 20 °C with an osmotic work of only about 0.05 kT per DOPE molecule. The low enthalpy also implies that the transition will be sensitive to changes in other system variables as well, variables that might otherwise be considered to be of only secondary importance. These may act at either the polar or the hydrocarbon regions of the assemblies. For example, charged lipids might sense salt concentration, pH, or particular binding ions in influencing phase transformations. Indeed, small polar molecules like trehalose (Wistrom et al., 1989), salt concentration (Seddon et al., 1983), polar group methylation (Gruner et al., 1988), proteins (Gulik-Krzywicki, 1975), and apolar molecules like alkanes, in small amounts (Kirk et al., 1984), have all been shown to influence these phase transitions. All such factors could be determinants in modifying stress within bilayers or in effecting the structural rearrangements that occur in the fusion of cell membranes.

The lipid monolayers of these phases are subject to many geometry-dependent free energy contributions whose magnitudes may change sharply at mesomorphic transitions. In undergoing an H_{II} to L_α transition, many structural features of the system change: The headgroup area expands while the area at the ends of the tails shrinks; the hydrocarbon chain environment is different as reflected by a decrease in $C-H_2$ bond orientational order parameters (Lafleur et al., 1990); the shape and distribution of the water volume change dramatically; etc. These changes may be accompanied by shifts in free energies associated with headgroup interactions, with the packing of the chains, and with interactions with water and solutes, etc. We simply do not understand enough about the functional dependence of these contributions on the mesomorphic geometry to assess the relative importance of each.

There is still much that is unknown about even the relatively simple DOPE/water system. Any dramatic progress in understanding the interactions active in the much more complicated multicomponent systems which characterize biological membranes is unlikely without a better understanding of the same interactions in simpler, more readily manipulated model systems.

Acknowledgments

We thank Erramilli Shyamsunder and David Turner for useful comments. The help of Norman Gershfeld (Bethesda, MD) and Alfred Möps (Leipzig, Germany) in the calorimetry experiments is appreciated. K.G. thanks the "NMR in vivo Center" of NIH for providing the Bruker MSL 300 spectrometer.

Registry No. DOPE, 4004-05-1.

References

Arnold, K., Pratsch, L., & Gawrisch, K. (1983) *Biochim. Biophys. Acta 728*, 121–128.

Boni, L. T., Stewart, T. P., & Hui, S. W. (1984) *J. Membr. Biol. 80*, 91–104.

Charvolin, J. (1990) *Contemp. Phys. 31*, 1–17.

Davis, J. H., Jeffrey, K. R., Bloom, M., Valic, M. I., & Higgs, T. P. (1976) *Chem. Phys. Lett. 42*, 390–394.

Epand, R. M. (1985) *Biochemistry 24*, 7092–7095.

Gawrisch, K., Arnold, K., Dietze, K., & Schulze, U. (1988) in *Electromagnetic Fields and Biomembranes* (Markov, M., & Blank, M., Eds.) pp 9–18, Plenum Press, New York.

Gruner, S. M. (1985) *Proc. Natl. Acad. Sci. U.S.A. 82*, 3665–3669.
Gruner, S. M. (1989) *Biophys. J. 56*, 1045–1049.
Gruner, S. M., Rothschild, K. J., & Clark, N. A. (1982) *Biophys. J.*, 241–251.
Gruner, S. M., Parsegian, V. A., & Rand, R. P. (1986) *Faraday Discuss. Chem. Soc. 81*, 29–37.
Gruner, S. M., Tate, M. W., Kirk, G. L., So, P. T. C., Turner, T. C., Keane, D. T., Tilcock, C. P. S., & Cullis, P. R. (1988) *Biochemistry 27*, 2853–2866.
Gulik-Krzywicki, T. (1975) *Biochim. Biophys. Acta 415*, 1–28.
Helfrich, W. (1973) *Z. Naturforsch. 28C*, 693–703.
Kirk, G. L., & Gruner, S. M. (1985) *J. Phys. (Paris) 46*, 761–769.
Kirk, G. L., Gruner, S. M., & Stein, D. L. (1984) *Biochemistry 23*, 1093–1102.
Kozlov, M. M., & Winterhalter, M. (1991a) *J. Phys. II France 1*, 1077–1184.
Kozlov, M. M., & Winterhalter, M. (1991b) *J. Phys. II France 1*, 1085–1100.
Lafleur, M., Cullis, P. R., Fine, B., & Bloom, M. (1990) *Biochemistry 29*, 8325–8333.
Luzzati, V. (1968) in *Biological Membranes* (Chapman, D., Ed.) pp 71–123, Academic Press, New York.
Luzzati, V., & Husson, F. (1962) *J. Cell Biol. 12*, 207–219.
Mabrey, S., & Sturtevant, J. M. (1976) *Proc. Natl. Acad. Sci. U.S.A. 73*, 3862–3866.
Parsegian, V. A., Rand, R. P., Fuller, N. L., & Rau, D. C. (1986) *Methods Enzymol. 127*, 400–416.
Rance, M., & Byrd, R. A. (1983) *J. Magn. Reson. 52*, 221–240.
Rand, R. P., & Parsegian, V. A. (1989) *Biochim. Biophys. Acta 988*, 351–376.
Rand, R. P., Fuller, N. L., Gruner, S. M., & Parsegian, V. A. (1990) *Biochemistry 29*, 76–87.
Rigaud, J. L., Gary-Bobo, C. M., & Lange, Y. (1972) *Biochim. Biophys. Acta 266*, 72–84.
Seddon, J. M. (1990) *Biochim. Biophys. Acta 1031*, 1–69.
Seddon, J. M., Cevc, G., & Marsh, D. (1983) *Biochemistry 22*, 1280–1289.
Tate, M. W., & Gruner, S. M. (1989) *Biochemistry 28*, 4245–4253.
Tate, M. W., Shyamsunder, E., Gruner, S. M., & D'Amico, K. L. (1991) *Biochemistry* (in press).
Tilcock, C. P. S., & Cullis, P. R. (1982) *Biochim. Biophys. Acta 684*, 212–222.
Turner, D. C. (1990) Ph.D. Thesis, Princeton University.
Turner, D. C., & Gruner, S. M. (1989) *Biophys. J. 55*, 116a.
Turner, D. C., & Gruner, S. M. (1991) *Biochemistry* (in press).
Wistrom, C. A., Rand, R. P., Growe, L. M., Spargo, B. J., & Crowe, J. H. (1989) *Biochim. Biophys. Acta 984*, 238–242.